Measurement of angular distribution and polarization of photon-induced fluorescent x rays in thorium and uranium

K. S. Kahlon, H. S. Aulakh, N. Singh, R. Mittal, K. L. Allawadhi, and B. S. Sood
Nuclear Science Laboratories, Physics Department, Punjabi University, Patiala 147 002, India
(Received 15 June 1990)

The angular distribution and polarization of the L-shell fluorescent x rays excited by 59.57-keV photons in Th and U have been measured. It is found that the $L\gamma$ group of L x rays is isotropic in spatial distribution and unpolarized but, the Ll and $L\alpha$ groups are anisotropically distributed and are polarized. Although no anisotropy of the $L\beta$ group is detected, it is found to be slightly polarized. The present results contradict the predictions of the calculations of Cooper and Zare [*Atomic Collision Processes* (Gordon and Breach, New York, 1969)] that after photoionization the magnetic substates of all subshell vacancy states are equally populated. However, the present results confirm the predictions of Flügge, Mehlhorn, and Schmidt [Phys. Rev. Lett. **29**, 7 (1972)] that the population distribution of the magnetic substates of all subshell vacancy states with $j > \frac{1}{2}$ is nonstatistical.

INTRODUCTION

The angular distribution and polarization of K- and L-shell x rays emitted from different elements when bombarded with various types of ions have been extensively studied,[1,2] but very little work has been reported on similar studies on x rays following photoionization. Generally, the observed spatial anisotropy and polarization of x rays and Auger electrons emitted on decay of vacancy states produced in ion-atom collisions show agreement with theoretical calculations. However, theoretical predictions of angular distribution and polarization of x rays emitted after photoionization are contradictory and need experimental verification.

The calculations of Cooper and Zare[3] predicted that after photoionization the inner-shell vacancy states have an equal population of magnetic substates and the radiation emitted subsequent to the decay of vacancies is therefore expected to be isotropic in the spatial distribution and unpolarized. However, later calculations by Flügge, Mehlhorn, and Schmidt[4] do not fully confirm these expectations but show that, if the total angular momentum j of the vacancy state after photoionization is greater than $\frac{1}{2}$, the population of its magnetic substates is nonstatistical. Thus, according to Flugge, Mehlhorn, and Schmidt,[4] after photoionization, the fluorescent x rays originating from the vacancy states with $j=\frac{1}{2}$ (K shell and L_1, L_2, M_1, and M_2 subshells etc.) will only be isotropic and unpolarized, but those fluorescent x rays which are emitted from the filling of vacancy states with $j=\frac{3}{2}$ (L_3, M_3, and M_4 subshells) and with $j=\frac{5}{2}$ (M_5 subshell) will only be anisotropic and polarized.

In order to test the theoretical calculations we have measured the differential cross sections for the emission of Ll, $L\alpha$, $L\beta$, and $L\gamma$ x rays of thorium and uranium by 59.57-keV γ rays in the angular range 40°–120° at intervals of 10°. We have also measured the linear polarization of Ll, $L\alpha$, $L\beta$, and $L\gamma$ x rays emitted at 90° with an x-ray polarimeter using coherent scattering as the analyzing process.

DIFFERENTIAL CROSS-SECTION MEASUREMENTS

The experimental arrangement used to measure differential cross sections for the emission of L x rays of Th and U is shown in Fig. 1. The ^{241}Am source S, the Th or U target T, and the Si(Li) detector D are arranged on a graduated turntable. Since the detector D is heavy and fragile it is kept fixed at one position, while the source S and target T are mounted on a moveable arm which can rotate about an axis through the center 0 of the table and move the source and target together with respect to detector to change angle STD without changing source-target solid angle. The shielding is so arranged that γ rays emitted from the source are made to fall on the target, and the radiation emitted from the target at angle θ after the interaction of γ rays with it are collimated on the detector. The angle of incidence is kept fixed at 70°,

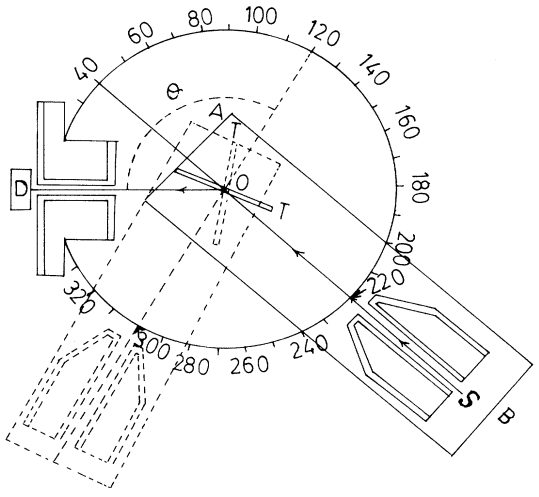

FIG. 1. Experimental set up used for the measurement of differential cross sections for the emission of L x rays after photoionization in Th and U. S is the radioactive source ^{241}Am; T is the target; D is the detector Si(Li).

while the angle at which the fluorescent x rays emitted from the target are detected is varied from 40° to 120°, with an angular spread of ±2.5° by rotating the movable arm. The limits on the angles are imposed by the sizes of collimators and distances of source and detector from the target; these are so adjusted that a signal-to-background ratio of 1000:1 is obtained. 59.57-keV γ rays from the ^{241}Am source of strength approximately 100 mCi are made to fall, in turn, on 99.99% pure metallic Th and U targets of diameter 4 cm and induce L-shell fluorescent x rays in it due to the photoionization of L-shell electrons. The K-shell electrons of Th and U are not ionized since their K-edge energies are higher than 59.57 keV. Therefore there is not transfer of vacancies from the K to the L shell, and the emission of L-shell fluorescent x rays from the target is entirely due to the photoionization of L-shell electrons by the incident photons. The population distribution of the various L-shell vacancy states produced by photoionization is thus not disturbed due to the transfer of vacancies from the K to the L shell. However, the Coster-Kronig transitions will alter the population distribution of the vacancies among various subshells by the factor K given by

$$K=\frac{\sigma_{L_3}}{\sigma_{L_3}+f_{23}\sigma_{L_2}+(f_{13}+f_{12}f_{23})\sigma_{L_1}}\ , \tag{1}$$

where σ_{L_i} $(i=1,2,3)$ are the L_i subshell photoionization cross sections and fij are the Coster-Kronig transition probabilities.

The fluorescent x rays emitted from the targets at an angle θ with the incident beam are analyzed and counted with the Si(Li) detector (effective area 200 mm^2, thickness 5 mm, Be window thickness 0.05) coupled to the ND 76 multichannel analyzer system. The resolution of the x-ray spectrometer is approximately 300 eV at 5.9 keV. A typical L x-ray spectrum of uranium taken at 90° is shown in Fig. 2. The peaks due to the Ll, $L\alpha$, $L\beta$, and $L\gamma$ groups of lines are well resolved. The differential cross sections for the emission of an L x ray under the L_i peak $(i=l,\alpha,\beta,\gamma)$ at angle θ is given by

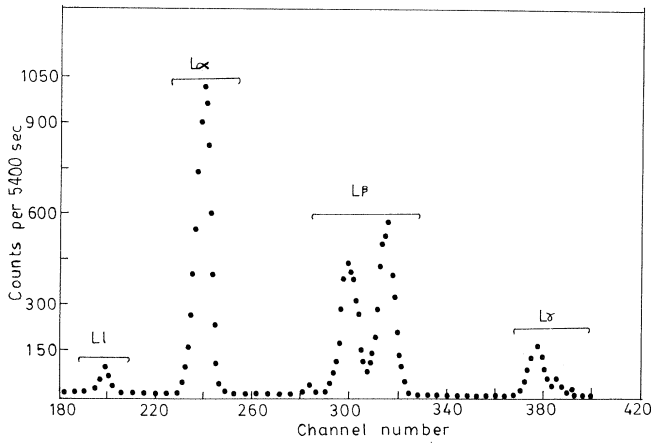

FIG. 2. Spectrum of U L x rays recorded with Si(Li) x-ray spectrometer at an emission angle of 90°.

$$\frac{d\sigma^{\theta}(L_i)}{d\Omega}=N_x^{\theta}(L_i)\frac{M}{N}\frac{1}{t\beta^{\theta}(L_i)}\left[\frac{4\pi}{S(\gamma)a(\gamma)w_1w_2^{\theta}\epsilon^{\theta}(L_i)}\right], \tag{2}$$

where $N_x^{\theta}(L_i)$ is the number of L x rays detected per second under the L_i x ray peak at an angle θ with incident γ ray beam; M is the atomic weight of Th and U in grams; N is Avogadro's number; t is thickness of the target in g/cm^2; $\beta^{\theta}(L_i)$ is the target self-absorption correction factor, which takes into account the absorption of incident γ rays and emitted x rays in the target; $S(\gamma)$ is the number of 59.57-keV γ rays emitted per second from the source; and $a(\gamma)$ is the correction due to the absorption of γ rays in an air column between source and target. w_1 and w_2 are the source-target and target-detector solid angles and $\epsilon^{\theta}(L_i)$ is the efficiency of the detector for the detection of x rays emitted at angle θ under the L_i x-ray peak. w_1 is independent of θ since angle of incidence is kept fixed throughout the experiment, but $N_x^{\theta}(L_i)$, $\beta^{\theta}(L_i)$, and $\epsilon^{\theta}(L_i)$ are dependent upon θ. Therefore, for the measurement of differential x-ray emission cross sections, the values of $N_x^{\theta}(L_i)$, $\beta^{\theta}(L_i)$, w_2^{θ}, and $\epsilon^{\theta}(L_i)$ have to be determined at each angle. $N_x^{\theta}(L_i)$ was measured from the total number of counts observed per unit time under the Ll, $L\alpha$, $L\beta$, and $L\gamma$ peaks in x-ray spectra taken at various angles varying from 40° to 120° at intervals of 10°. The terms M/Nt and $\beta^{\theta}(L_i)$ were calculated from the physical parameters of the target and the absorption coefficients of incident γ rays and emergent x rays in Th and U, respectively. Since the emergent x rays under each of the L_i peaks consists of a number of x-ray lines of distinct energies and intensities, the values of $\beta^{\theta}(L_i)$ at different angles of emergence used in the experiment were calculated by the procedure described earlier.[5] The values of the factor $4\pi/S(\gamma)a(\gamma)w_1w_2^{\theta}\epsilon^{\theta}(L_i)$, which contains terms relating to the γ-ray source strength, source-target and target-detector solid angles, and detector efficiency were determined experimentally for various emission angles and different x-ray energies ranging from 6 to 26 keV in terms of K x-ray production cross sections, which are known to an accuracy of approximately 1–2 %. For this purpose Th and U targets were replaced, in turn, with targets of Fe, Ni, Cu, Ge, Se, Y, Zr, Mo, Ag, and Sn, and the intensity of K x rays emitted from each of the targets at different angles was recorded. A typical spectrum of K x-rays emitted from the target of Ge at an angle of 90° is shown in Fig. 3. It can be easily seen that the factor under reference

$$\frac{4\pi}{S(\gamma)a(\gamma)w_1w_2^{\theta}\epsilon^{\theta}(L_i)}=\frac{\sigma_K}{4\pi}\frac{1}{N_x^{\theta}(L_i)}\frac{N}{M}t_K\beta^{\theta}(K)\ , \tag{3}$$

where various terms have the same meaning as explained in Eq. (2) but correspond to the K shell and are evaluated as explained above. The isotropic emission of K x rays, which has been verified experimentally, is assumed. The values of the factor for different emission angles at the weighted mean energies of the K x rays of the elements of various targets with atomic number $26\leq Z<\leq 50$ were determined from Eq. (3). The values of the factor corre-

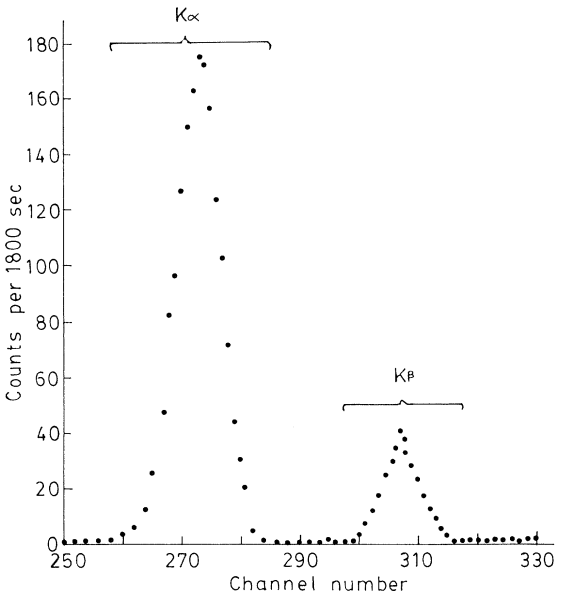

FIG. 3. Spectrum of Ge K x rays recorded with Si(Li) x-ray spectrometer at an emission angle of 90°.

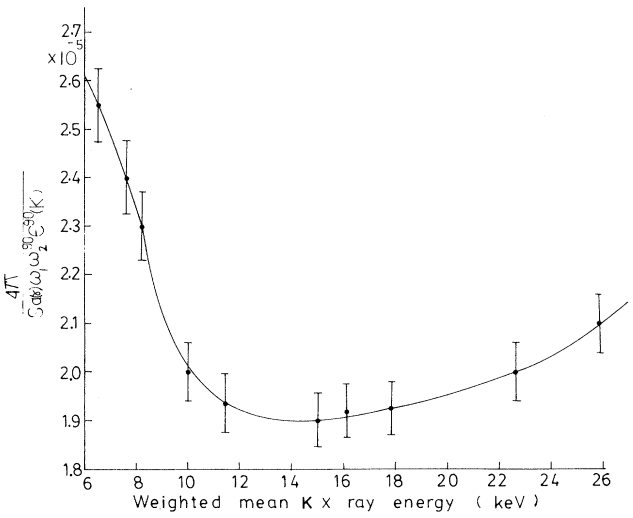

FIG. 4. Values of the factor $4\pi/s(\gamma)a(\gamma)w_1w_2^{90}\epsilon^{90}(L_i)$ at the weighted mean K x-ray energies of the elements $26 \leq Z \leq 50$.

sponding to emission angle of 90° are shown in Fig. 4. The values of the factor for various emission angles at the weighted mean energies corresponding to Ll, $L\alpha$, $L\beta$, and $L\gamma$ groups of L x-ray lines were determined from the figures similar to Fig. 4 for the evaluation of differential cross sections $d\sigma^{\theta}(L_i)/d\Omega$ from Eq. (2).

The measured values of differential cross sections for the emission of Ll, $L\alpha$, $L\beta$, and $L\gamma$ groups of L x-ray lines at different emission angles varying from 40° to 120° are shown in Table I. To the best of our knowledge, no other experimental data are available for comparison with present results. The errors in the present measurements are 6–8 % and are due to counting statistics and the uncertainties involved in calculations and/or measurement of other parameters used for the determination of the x-ray emission cross sections from Eq. (1). It is seen from the results that $L\beta$ and $L\gamma$ peaks are emitted isotropically, while Ll and $L\alpha$ peaks show anisotropic emission. The anisotropy of Ll peak is more than that of

TABLE I. Measured differential L_i x-ray emission cross sections ($i = l$, α, β, and γ).

Emission angle θ	$\frac{d\sigma^{\theta}(Ll)}{d\Omega}$	$\frac{d\sigma^{\theta}(L\alpha)}{d\Omega}$	$\frac{d\sigma^{\theta}(L\beta)}{d\Omega}$	$\frac{d\sigma^{\theta}(L\gamma)}{d\Omega}$
		U		
40°	3.74±0.22	37.80±2.6	37.80±2	8.83±0.45
50°	3.34±0.20	36.61±2.5	38.04±2	8.75±0.45
60°	2.95±0.18	35.33±2.4	38.20±2	8.75±0.45
70°	2.63±0.16	34.62±2.4	38.50±2	9.07±0.47
80°	2.31±0.14	33.66±2.3	38.00±2	8.91±0.46
90°	2.07±0.12	32.47±2.2	38.20±2	8.83±0.45
100°	1.83±0.11	31.19±2.1	38.00±2	8.91±0.46
110°	1.59±0.10	30.24±2.0	38.00±2	8.75±0.45
120°	1.32±0.08	29.44±2.0	38.30±2	8.83±0.45
		Th		
40°	2.47±0.15	30.80±2.10	34.93±1.8	5.89±0.53
50°	2.28±0.14	29.76±2.10	35.07±1.8	6.13±0.55
60°	2.07±0.13	28.65±2.00	35.09±1.8	6.13±0.55
70°	1.95±0.12	27.53±2.00	35.17±1.8	5.89±0.53
80°	1.77±0.10	26.65±2.00	34.85±1.8	6.05±0.54
90°	1.67±0.09	26.10±1.80	35.01±1.8	6.01±0.54
100°	1.51±0.09	25.15±1.80	34.62±1.7	5.93±0.53
110°	1.40±0.09	24.35±1.70	34.85±1.8	6.13±0.55
120°	1.27±0.08	22.92±1.60	34.78±1.8	6.21±0.56

$L\alpha$ peak. According to the calculation of Flügge, Mehlhorn, and Schmidt,[4] Ll and $L\alpha$ peaks are expected to show anisotropic emission because both of them originate from transitions to the L_3 ($J=\frac{3}{2}$) subshell. The observed anisotropy of $L\alpha$ peak is less than that of Ll peak because $L\alpha$ peak contains $L\alpha_1(L_3-M_5)$ and $L\alpha_2(L_3-M_4)$ lines of opposite anisotropy, but Ll peak contains only one intense line (L_3-M_1). However, even though the $L\beta$ peak contains some contribution from L_3 ($J=\frac{3}{2}$) subshell transitions in addition to those from L_1 and L_2 subshells with $J=\frac{1}{2}$, it does not show any measurable anisotropy. Thus the $L\beta$ peak may also be taken to be isotropically emitted within the uncertainties of present measurements. The $L\gamma$ peak consists of the transition only from L_1 ($j=\frac{1}{2}$) and L_2 ($J=\frac{1}{2}$) subshells and is thus expected to be isotropically emitted. Representing the differential x-ray emission cross sections for any group (L_i) of L x-ray lines by a Legendre polynomial sum

$$\frac{d\sigma^\theta}{d\Omega}(L_i)=\sum_l a_l P_l(\cos\theta) ,$$

the observed cross-sections are fitted to the relation

$$\frac{d\sigma^\theta}{d\Omega}(L_i)=a_0+a_1\cos\theta+a_2\cos^2\theta .$$

The values of the coefficients a_0, a_1, and a_2 are listed in Table II. The experimental values of differential cross sections and the fitted curves are shown in Figs. 5 and 6.

Since the values of theoretical angular distribution function for the emission of Ll, $L\alpha$, $L\beta$, and $L\gamma$ groups of lines are not available in literature, the experimental differential cross sections had to be converted to integral cross sections for the comparison of the present results with theory. The integral cross sections for the emission of L_i groups of L x rays were found by using the relation

$$\sigma_{\text{tot}}=2\pi\int_0^\pi \frac{d\sigma^\theta}{d\Omega}(L_i)\sin\theta\, d\theta .$$

The integral emission cross section for the Ll, $L\alpha$, $L\beta$, and $L\gamma$ groups were calculated from the theoretical values of L-subshell photoionization cross sections, radiative decay rates, semiempirical fitted values of fluorescence yields, and Coster-Kronig transition probabilities using the following relations:

TABLE II. Experimental values of coefficients a_l $l=0,1,2$.

Element	L x-ray group	Coefficient a_l a_0	a_1	a_2
U	Ll	2.07	1.61	0.57
	$L\alpha$	32.47	6.51	−0.103
	$L\beta$	38.12	0	0
	$L\gamma$	8.85	0	0
Th	Ll	1.67	0.86	0.19
	$L\alpha$	26.10	5.32	0.61
	$L\beta$	34.93	0	0
	$L\gamma$	6.20	0	0

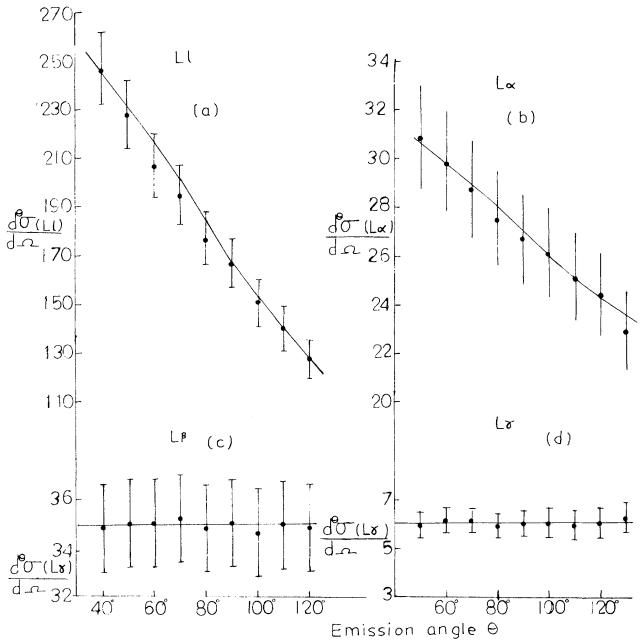

FIG. 5. Differential L-shell x-ray emission cross section of Th at angles from 40° to 120°: (a) $(d\sigma^\theta/d\Omega)(Ll)$ vs θ, (b) $(d\sigma^\theta/d\Omega)(L\alpha)$ vs θ, (c) $(d\sigma^\theta/d\Omega)(L\beta)$ vs θ, and (d) $(d\sigma^\theta/d\Omega)(L\gamma)$ vs θ.

$$\sigma^x_{Ll}=[\sigma_1(f_{13}+f_{12}f_{23})+\sigma_2 f_{23}+\sigma_3]w_3F_{3l} ,$$

$$\sigma^x_{L\alpha}=[\sigma_1(f_{13}+f_{12}f_{23})+\sigma_2 f_{23}+\sigma_3]w_3F_{3\alpha} ,$$

$$\sigma^x_{L\beta}=\sigma_1 w_1F_{1\beta}+(\sigma_1 f_{12}+\sigma_2)w_2F_{2\beta}$$
$$+[\sigma_3+\sigma_2 f_{23}+\sigma_1(f_{13}+f_{12}f_{23})]w_3F_{3\beta} ,$$

$$\sigma^x_{L\gamma}=\sigma_1 w_1F_{1\gamma}+(\sigma_2+\sigma_1 f_{12})w_2F_{2\gamma} ,$$

where σ_1, σ_2, and σ_3 are L-subshell photoionization cross sections of the element under investigation; w_1, w_2, and

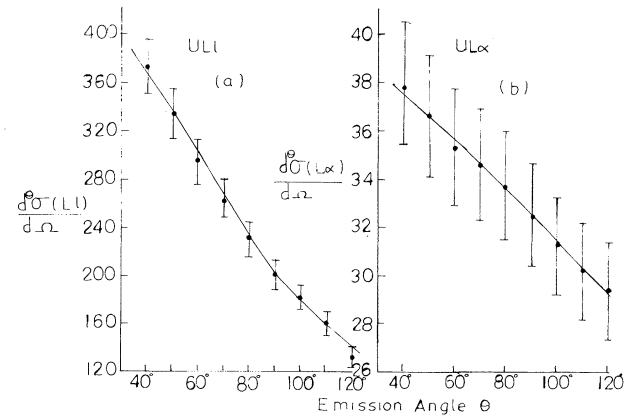

FIG. 6. Differential L-shell x-ray emission cross section of U at angles from 40° to 120°: (a) $(d\sigma^\theta/d\Omega)(Ll)$ vs θ and (b) $(d\sigma^\theta/d\Omega)(L\alpha)$ vs θ.

TABLE III. Comparison of experimental and calculated values of integral cross sections.

Element	L x-ray group	Measured values	Calculated values
Th	Ll	21.4±1	21
	$L\alpha$	334±17	342
	$L\beta$	439±18	440
	$L\gamma$	78±3	81
U	Ll	28±1.4	26
	$L\alpha$	408±20	407
	$L\beta$	479±19	496
	$L\gamma$	111±3	113

w_3 are the subshell fluorescence yields; f_{13}, f_{12}, and f_{23} are the intra-L-subshell Coster-Kronig transition probabilities, and the F's are the fractional radiative decay rates, e.g., F_{3l} is the fraction of L_{III} subshell x rays which contribute to Ll peak of the x-ray spectrum of an element. The experimental and calculated integral cross sections are compared in Table III and are found to show good agreement with each other.

POLARIZATION MEASUREMENTS

The linear polarization of the L-shell x rays excited by 59.57-keV γ rays in Th and U was measured with an x-ray polarimeter using coherent scattering as the analyzing process. The L-shell x rays whose polarization is to be determined are scattered from a carbon scatterer and the intensity of the coherent scattering at 90° is measured in turn, in the x-ray emission plane (i.e., plane containing incident γ rays and emitted x rays) and perpendicular to it, respectively. The experimental set up is shown in Fig. 7. A collimated beam of 59.57-keV γ rays from approximately 100-mCi ^{241}Am source S is allowed to fall, in turn, on targets T of Th and U and the L-shell fluorescent x rays emitted from them at 90° are again collimated on a carbon scatterer C and allowed to scatter from it at 90°

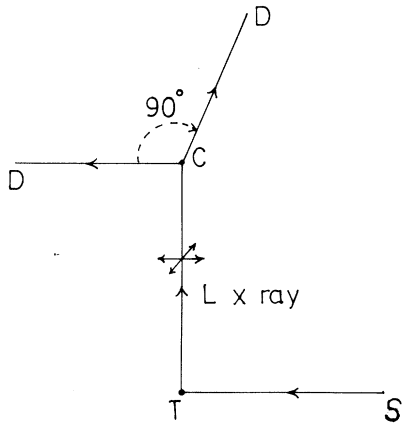

FIG. 7. Experimental setup used for the measurement of L x-ray polarization in Th and U. S is the radioactive source ^{241}Am; T is the target (Th and U); C is the carbon scatterer; D is the detector Si(Li).

into detector D, which is kept first in the x-ray emission plane and then along a direction perpendicular to it. The detector D is so shielded that it can only receive scattered x rays from the carbon scatterer.

The radiation falling on the carbon scatterer consists of L, M, and higher-L-shell fluorescent x rays of Th and U and the coherent and incoherent scattering of 59.57-keV γ rays. The K-shell x rays of Th and U are not excited because the K edges of Th and U are higher than 59.57 keV. The L-shell x rays are easily isolated from the scattering by the Si(Li) detector described earlier in the cross-section measurements. The spectrum of radiation in the energy range 10–20 keV falling on the carbon scatterer when Th target is irradiated with 59.57-keV γ rays is shown in Fig. 8(a). The peaks corresponding to Ll, $L\alpha$, $L\beta$, and $L\gamma$ groups of L x rays of Th are clearly seen. The polarization of x rays falling under the Ll, $L\alpha$, $L\beta$, and $L\gamma$ peaks is analyzed by the method described earlier.[6] It consists of determining the sensitivity R of the polarimeter and measuring the counting rates $N_{\parallel}$ and $N_{\perp}$ under the Ll, $L\alpha$, $L\beta$, and $L\gamma$ peaks in the spectra of radiation scattered from the carbon scatterer at 90° when the scatterer-detector line CD is parallel and perpendicular to x-ray emission plane, respectively. The spectra of the L-shell radiation of Th scattered from the carbon scatterer in the two mutually perpendicular directions are shown in Fig. 8(b). It is seen that the areas under each of the Ll, $L\alpha$, and $L\beta$ peaks observed in the two directions are different, but that under the $L\gamma$ peak they are almost the same in both directions; this clearly indicates that the radiation observed under the Ll, $L\alpha$, and $L\beta$ peaks is polarized, but that under the $L\gamma$ peak is unpolarized. In order to ensure that the x-ray detector and shielding used

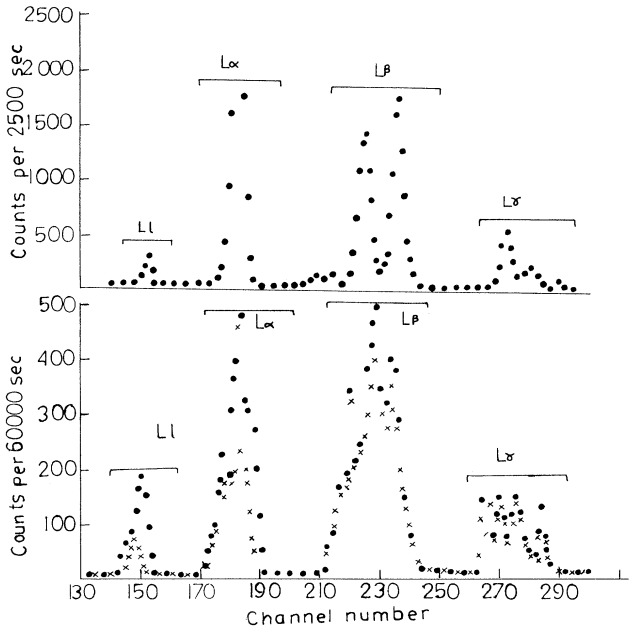

FIG. 8. (a) Spectrum of Th L x rays falling on the scatterer C. (b) Spectrum of Th L x rays after scattering from the carbon scatterer. ● corresponds to the detector in the x-ray emission plane, × corresponds to the detector placed perpendicular to the emission plane.

TABLE IV. Experimental values of percentage polarization.

Peak	$N_{\parallel}/N_{\perp}$ Th	$N_{\parallel}/N_{\perp}$ U	Percentage polarization $P=(R+1)(N_{\parallel}-N_{\perp})/(R-1)(N_{\parallel}+N_{\perp})\times 100$ Th	U
Ll	2.29±0.11	2.14±0.11	86±6	79±6
$L\alpha$	1.32±0.05	1.40±0.06	29±2	36±2
$L\beta$	1.04±0.04	1.13±0.05	4±.03	13±0.8
$L\gamma$	1.02±0.05	1.01±0.05	1±0.09	1±0.09

in the polarimeter arrangement are symmetrical about the axis TC, and the observed differences in the intensities of x-ray scattering from the carbon scatterer measured in two mutually perpendicular directions are not due to any asymmetry of the geometry, two experimental tests are performed. In the first test, the strong ^{241}Am source S and target T used in the main experiment are removed and a weak ^{241}Am is placed at the position of the target T. The intensities of the scattering of the unpolarized beam of 59.57-keV γ rays at 90° from carbon scatterer, when measured in the two perpendicular directions, are found to be equal within statistics, thus showing the symmetry of the polarimeter arrangement. In the second test experiment Mo is used as the target T instead of Th and U, and the scattering of its unpolarized K x rays from C is measured and found to be equal within statistics in both the directions, thus confirming the symmetry of the geometry. It may be noted that the observed equality and inequality of scattered counts in the two directions for $L\gamma$ group and each of the Ll, $L\alpha$, and $L\beta$ groups, respectively, also indirectly shows the symmetry of the polarimeter shielding.

As explained earlier the percentage polarization is given as

$$P=\frac{(N_{\parallel}/N_{\perp}-1)(R+1)}{(N_{\parallel}/N_{\perp}+1)(R-1)}\times 100 .$$

The sensitivity of the polarimeter R, which is defined for the plane polarized radiations incident on the carbon scatterer C as the ratio of $N_{\parallel}/N_{\perp}$ of the counting rates in the two mutually perpendicular extreme positions of the detector (i.e., one parallel and the other perpendicular to the x-ray emission plane) was determined experimentally by the method described earlier.[6] The polarization of the coherent scattering of 59.57-keV γ rays from the Th target at 90° having 100% polarization was analyzed in terms of the ratio $N_{\parallel}/N_{\perp}$, and the value of R was found to be 2.67±0.04 for the spread involved in the angle of x-ray emission from the target T and the angle of scattering from the carbon scatterer C in the present measurements. The counting rates involved in the measurements were rather low and the experiment had to be run for several weeks to get good statistics. The equipment was calibrated periodically to keep a check on its stability. The constancy of data provided an indirect check on stability.

The final results are given in Table IV, which gives the values of $N_{\parallel}/N_{\perp}$ and the percentage of polarization for L-shell fluorescent x rays observed under different peaks. The errors shown are the probable errors in the final results.

CONCLUSIONS

The present experimental results show that in the fluorescent L x-ray emission spectra of Th and U by 59.57-keV γ rays, the L groups which contain x-ray lines from the filling of vacancies in the L_1 and L_2 subshells with $j=\frac{1}{2}$ are emitted isotropically and are unpolarized, whereas the Ll and $L\alpha$ groups consisting of x-ray lines from the vacancy filling in the L_3 subshell with $j=\frac{3}{2}$ only show anisotropic emission and linear polarization with the electric vector perpendicular to the x-ray emission plane. The $L\beta$ group that contains x-ray lines from all the three L_1, L_2, and L_3 subshells does not show any significant anisotropy which could be detected within the accuracy of the present measurements, but it does manifest some linear polarization. The observed anisotropy and the percentage polarization for Ll group are higher than the $L\alpha$ group, which is explained from the fact that the Ll group contains only one intense line (L_3-M_1), but the $L\alpha$ group consists of $L\alpha_1$ (L_3-M_5) and $L\alpha_2$ (L_3-M_4) lines, which have opposite anisotropy and polarization.

It is concluded that the present results contradict the predictions of the calculations of Cooper and Zare[3] that after photoionization the magnetic substates of all the vacancy states, irrespective of their j values, are equally populated and are thus unaligned; however, they confirm those of Flügge, Mehlhorn, and Schmidt[2] that all the vacancy states with $j>\frac{1}{2}$ have a nonstatistical population distribution of their magnetic substates and are aligned.

ACKNOWLEDGMENTS

The financial assistance from Department of Science and Technology and University Grants Commission is gratefully acknowledged.

[1]T. Papp and J. Palinkas, Phys. Rev. A **38**, 2686 (1988).
[2]S. C. McFarlane, J. Phys. B **5**, 1906 (1972).
[3]J. Cooper and R. N. Zare, *Atomic Collision Processes* (Gordon and Breach, New York, 1969), Vol. X1 C 317.
[4]S. Flügge, W. Mehlhorn, and V. Schmidt, Phys. Rev. Lett. **29**, 7 (1972).
[5]S. K. Arora, K. L. Allawadhi, and B. S. Sood, J. Phys. B **14**, 1423 (1981).
[6]B. S. Sood, Proc. R. Soc. London Ser. A **247**, 375 (1958).